

Argonne National Laboratory, with facilities in the states of Illinois and Idaho, is owned by the United States Government and operated by The University of Chicago under the provisions of a contract with the Department of Energy.

DISCLAIMER

This report was prepared as an account of work sponsored by an agency of the United States Government. Neither the United States Government nor any agency thereof, nor The University of Chicago, nor any of their employees or officers, makes any warranty, express or implied, or assumes any legal liability or responsibility for the accuracy, completeness, or usefulness of any information, apparatus, product, or process disclosed, or represents that its use would not infringe privately owned rights. Reference herein to any specific commercial product, process, or service by trade name, trademark, manufacturer, or otherwise, does not necessarily constitute or imply its endorsement, recommendation, or favoring by the United States Government or any agency thereof. The views and opinions of document authors expressed herein do not necessarily state or reflect those of the United States Government or any agency thereof, Argonne National Laboratory, or The University of Chicago.

Available electronically at <http://www.doe.gov/bridge>

Available for a processing fee to U.S. Department of Energy and its contractors, in paper, from:

U.S. Department of Energy
Office of Scientific and Technical Information
P.O. Box 62
Oak Ridge, TN 37831-0062
phone: (865) 576-8401
fax: (865) 576-5728
email: reports@adonis.osti.gov

ANL-01/05

ARGONNE NATIONAL LABORATORY
9700 South Cass Avenue
Argonne, Illinois 60439

**Effect of Beam Interruptions on Liquid Metal Cooled
ATW Blanket Structures**

by

Floyd E. Dunn

January 2001

TABLE OF CONTENTS

	<u>Page</u>
ABSTRACT	vii
I. INTRODUCTION	1
II. OVERVIEW	2
III. ANALYSIS METHODS	4
A. The SASSYS-1 Plant Dynamics Code	4
B. Program TSLAB, One Dimensional Heat Conduction in Slab Geometry	4
C. Program TCYLNDNR, One Dimensional Heat Conduction in Cylindrical Geometry	4
D. Evaluation of Low Cycle Fatigue at Elevated Temperatures	5
E. Coolant Heat Transfer Coefficient	7
IV. RESULTS	9
A. Loss of Beam Transient	9
B. Impact of the Degree of Sub-Criticality	15
C. Beam Interruption Frequency Design Limits	15
V. MITIGATION OPTIONS	17
A. Improve the Reliability of the Accelerator	17
B. Sudden Return to Power	17
C. Pump Trip	18
D. Impact of Increased Thermal Impedance of the Fuel	21
E. Reducing the Core Coolant Temperature Rise	22
F. Eliminating the Above Core Load Pads	23
G. Summary of Mitigation Results	24
VI. FUTURE WORK	25
VII. SUMMARY AND CONCLUSIONS	26
APPENDIX A. VERIFICATION OF THE TSLAB CODE	27
REFERENCES	28

LIST OF FIGURES

	<u>Page</u>
1. Schematic of Coolant Flow in the ATW Blanket	3
2. TSLAB Geometry	5
3. Normalized Power and Flow, Beam Loss, No Pump Trip	9
4. Top of Core Coolant and Structure Temperatures (sodium coolant)	10
5. Top of Core Structure Average Temperature - Surface Temperature (sodium)	10
6. Outlet Plenum Temperatures (sodium)	11
7. Outlet Plenum Structure Average Temperature - Surface Temperature (sodium)	11
8. IHX Shell Temperatures (sodium)	12
9. IHX Shell Average Temperature - Surface Temperature (sodium)	12
10. IHX Upper Tube Sheet Temperatures (sodium)	13
11. IHX Tube Sheet Rim Outer Temperature - Tube Sheet Average Temperature (sodium)	13
12. Steam Generator Upper Tube Sheet Temperatures (Pb-Bi)	14
13. Tube Sheet Average Temperature - Surface Temperature (Pb-Bi)	14
14. Influence of k Effective on the Difference Between the Top of Core Structure Average Temperature - Surface Temperature	16
15. Temperature Differences in the Steam Generator Tube Sheet of a Lead-Bismuth Cooled ATW, Mitigation Options	18
16. Influence of Early Return to Power on the Top of Core Difference Between the Structure and the Coolant Temperatures	19
17. Impact of a Sudden Return to Power After Temperatures Have Equilibrated	19
18. Top of Core Temperatures After a Loss of Beam with a Pump Trip	20
19. Top of Core Structure Temperature - Coolant Temperature after a Loss of Beam	20
20. Outlet Plenum Temperatures After a Loss of Beam with a Pump Trip	20
21. Outlet Plenum Wall Temperature - Coolant Temperature After a Loss of Beam	20

LIST OF FIGURES

(Contd.)

	<u>Page</u>
22. Top of Core Structure Temperature Minus Coolant Temperature	21
23. Outlet Plenum Wall Temperature Minus Coolant Temperature	21
24. Temperature Differences in the Above Core Load Pads in the Sodium Cooled Case, Effect of Doubling the Coolant Flow Rate	23
25. Temperature Differences in the IHX Tube Sheet Rim in the Sodium Cooled Case, Effect of Doubling the Coolant Flow Rate	23
A1. Comparison of Exact and Finite Difference Solutions for a Slab Temperature Problem	27

LIST OF TABLES

	<u>Page</u>
1. Frequency of Beam Interruptions for the LANSCE Accelerator, as Compiled by Eriksson	1
2. Coolant Heat Transfer Coefficients Used in Structure Temperature Calculations	8
3. Estimates of Fatigue Damage Due to Beam Interruptions	15
4. Allowable Beam Interruption Frequencies for Current Blanket Designs	16
5. Results of Mitigation Actions	24

EFFECT OF BEAM INTERRUPTIONS ON LIQUID METAL COOLED ATW BLANKET STRUCTURES

by

Floyd E. Dunn

ABSTRACT

Thermal fatigue consequences of frequent accelerator beam interruptions are quantified for both sodium and lead-bismuth cooled blankets in current designs for accelerator transmutation of waste devices. Temperature response was calculated using the SASSYS-1 systems analysis code for an immediate drop in beam current from full power to zero. Coolant temperatures from SASSYS-1 were fed into a multi-node structure temperature calculation to obtain thermal strains for various structural components. Fatigue curves from the American Society of Mechanical Engineers Boiler and Pressure Vessel Code were used to determine the number of cycles that these components could endure, based on these thermal strains. Beam interruption frequency data from a current accelerator were used to estimate design lifetimes for components. Mitigation options for reducing thermal fatigue are discussed.

I. INTRODUCTION

In the past, accelerator design was focused on maximum particle energy or maximum beam power, rather than on continuous reliable operation for long periods of time. Frequent beam interruptions were tolerated as a price to be paid for maximum particle energy or maximum beam energy. For instance, Table 1 lists the frequency of beam interruptions for the LANSCE accelerator. In the past, power reactors were designed for constant power operation for long periods with no interruptions. The question that will be addressed in this report is whether these two technologies can be mated successfully. A beam interruption in an accelerator driven system is similar to a reactor scram, but faster. The specific areas addressed in this report are the thermal fatigue consequences of frequent beam interruptions in an accelerator driven system, and the mitigation options.

Table 1
Frequency of Beam Interruptions for the LANSCE Accelerator, as Compiled by Eriksson¹

Duration of interruption	Interruptions per day	Interruptions per year
10 seconds or more	39.0	14,200
1 minute or more	9.5	3,482
2 minutes or more	5.5	2,019
3 minutes or more	4.4	1,597
4 minutes or more	3.8	1,402
5 minutes or more	3.4	1,237
15 minutes or more	1.7	617
1 hour or more	0.6	214
5 hours or more	0.09	34

II. OVERVIEW

Thermal fatigue due to beam interruptions has been investigated in both sodium cooled and lead-bismuth cooled ATWs. For the sodium cooled case, the ALMR mod B design² was used as a basis for the subcritical source driven reactor. This is an 840 MW_{th} power plant. For the lead-bismuth case a similar design was used, but the intermediate heat exchanger was replaced by a once-through steam generator inside the reactor vessel, eliminating the intermediate coolant loop. Also, for the lead-bismuth case the core was replaced by a design by Yang³. In the lead-bismuth core the pins are smaller in diameter to give more coolant flow area and to give a lower core pressure drop.

Figure 1 shows a schematic of the coolant flow in the ALMR mod B design. The coolant flows upward through the core into an outlet plenum. From the outlet plenum the coolant flows directly into the shell side of the intermediate heat exchanger. In the intermediate heat exchanger the primary coolant flows downward and then out into a cold pool. From the cold pool the coolant is drawn into a pump and pumped back into the inlet plenum. The intermediate coolant flows upward through the tubes in the intermediate heat exchanger. It then flows through pipes to the steam generator and back to the intermediate heat exchanger. In the lead-bismuth case, the primary coolant flows downward on the shell side of the steam generator into the cold pool, and water and steam flow upward through the tubes in the steam generator. The steam from the steam generator flows through pipes to the turbine and the condenser. Then the condensed water is pumped back as feedwater to the steam generator.

Temperature response in the primary coolant system, and in the intermediate coolant system in the case of sodium coolant, was calculated, using the SASSYS-1 systems analysis code⁴, for an immediate drop in beam current from full power to zero. Coolant temperatures from SASSYS-1 were fed into a multi-node structure temperature calculation to obtain average temperatures and surface temperatures for the structures. Temperature differences were used to calculate thermal strains. Fatigue curves from the American Society of Mechanical Engineers Boiler and Pressure Vessel Code⁵ were used to determine the number of cycles that various components could endure, based on these thermal strains. The beam interruption frequency data of Table 1 were used to estimate the design lifetimes for the components.

The structural components considered in this work were the above-core load pads on the core subassembly walls, the upper part of the wall of the outlet plenum, the intermediate heat exchanger shell, the rim of the upper tube sheet in the intermediate heat exchanger, and the interior or the upper tube sheet in the steam generator. The upper part of the wall of the outlet plenum consists of a one inch thick vessel wall liner. Beyond the liner is an annulus of stagnant coolant, followed by the vessel wall. The vessel wall is two inches thick in the sodium coolant case. For the lead-bismuth case the vessel wall thickness was increased to four inches.

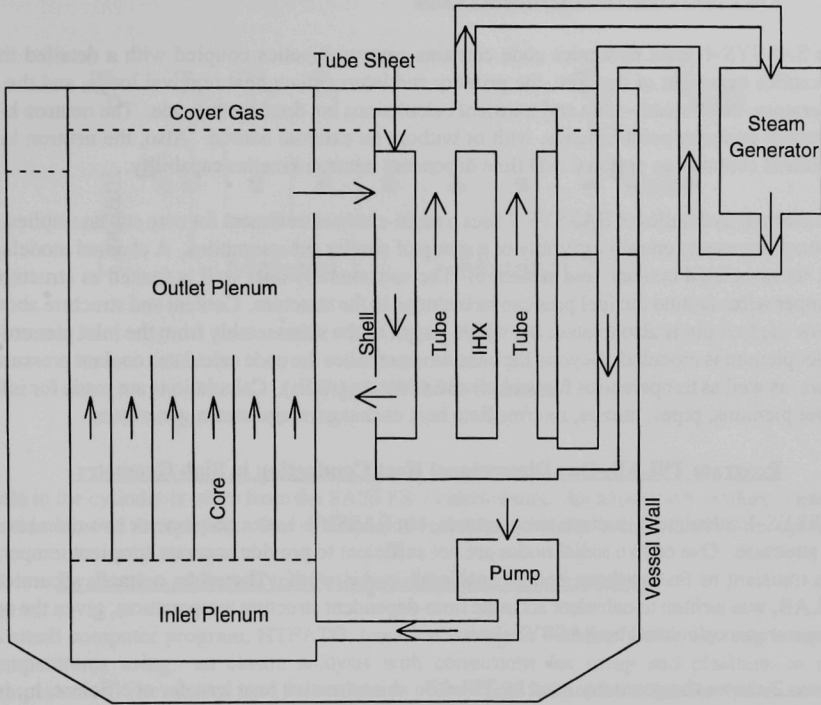


Fig. 1. Schematic of Coolant Flow in the ATW Blanket

III. ANALYSIS METHODS

A. The SASSYS-1 Plant Dynamics Code

The SASSYS-1 plant dynamics code contains neutron kinetics coupled with a detailed thermal hydraulics treatment of the core, the primary and intermediate heat removal loops, and the steam generators. Both steady-state and transient calculations are done by the code. The neutron kinetics treatment contains point kinetics, with or without an external source. Also, the neutron kinetics treatment contains an optional 3-D time dependent neutron kinetics capability.

The thermal hydraulics in SASSYS-1 uses a multi-channel treatment for core subassemblies. Each channel represents one subassembly or a group of similar subassemblies. A channel models a fuel pin, its associated coolant, and structure. The subassembly duct wall is treated as structure, and wrapper wires around the fuel pins can be included in the structure. Coolant and structure above and below the fuel pin is also treated: the whole length of the subassembly from the inlet plenum to the outlet plenum is modeled. Beyond the core subassemblies the code calculates coolant pressures and flows, as well as temperatures for coolant and structure (walls). Calculations are made for inlet and outlet plenums, pipes, pumps, intermediate heat exchangers, and steam generators.

B. Program TSLAB, One Dimensional Heat Conduction in Slab Geometry

SASSYS-1 calculates structure temperatures, but SASSYS-1 uses only one or two radial nodes in the structure. One or two radial nodes are not sufficient to provide accurate transient temperatures in a transient as fast as those being considered in this work. Therefore, a small, separate code, TSLAB, was written to calculate accurate time-dependent structure temperatures, given the coolant temperatures calculated by SASSYS-1.

Figure 2 shows the geometry used by TSLAB. A convective heat transfer coefficient, h_c , is used between the coolant temperature and the structure surface temperature, T_1 . Up to 50 temperature nodes are used within the structure. The structure can consist of a number of separate materials in contact with each other. Thus, when calculating temperatures in the outlet plenum wall, one can include the vessel wall liner, the annulus of stagnant coolant, and the vessel wall. It is also possible to account for a constant sink temperature, T_{sink} , and its associated heat transfer coefficient, h_{sink} , on the far side of the structure.

C. Program TCYLNDR, One Dimensional Heat Conduction in Cylindrical Geometry

In order to calculate temperature profiles within the tube sheets of the steam generators and the intermediate heat exchangers a small program, TCYLNDR, was written. The region around a tube penetration through the tube sheet is modelled as a cylinder with an inner radius equal to the inner radius of the tube. The outer radius of the cylinder is chosen to conserve the tube sheet volume associated with one tube. The time-dependent temperatures of the coolant going through the inner

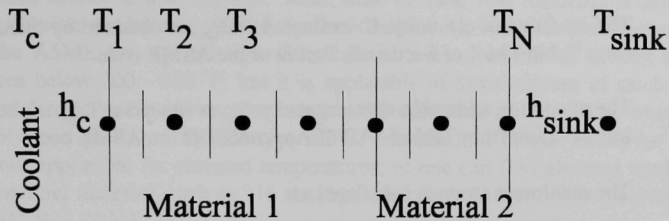


Fig. 2. TSLAB Geometry

hole in the cylinder is taken from the SASSYS-1 calculations. An adiabatic boundary is used at the outer radius of the cylinder. One dimensional radial heat transfer is calculated in the cylinder.

D. Evaluation of Low Cycle Fatigue at Elevated Temperatures

A small computer program, HTFATG, has been written to evaluate low cycle fatigue at elevated temperatures using an elastic analysis with corrections for creep and plasticity at elevated temperatures. The method used for evaluation of low cycle fatigue at elevated temperatures is based on article T-1432 of Appendix T of Subsection NH of the ASME Boiler and Pressure Vessel Code. This type of analysis is required when the temperatures exceed 700 or 800 °F. Appendix T only includes data for four materials: 304 stainless steel, 316 stainless steel, Ni-Fe-Cr alloy 800H, and 2 1/4 Cr-1 Mo steel. Any other material, such as HT-9, is not covered by this treatment.

In program HTFATG the user supplies the material type, the transient change in the temperature difference, ΔT , between the average temperature and the surface temperature, the lowest temperature in the transient, T_{low} , and the highest temperature during the transient, T_{high} .

The materials that can be used are 304 stainless steel, 316 stainless steel, Ni-Fe-Cr alloy 800H, and 2 1/4 Cr- 1Mo steel.

Then:

- 1) The thermal expansion coefficient, α , evaluated at T_{high} , is obtained by linear interpolation from Table TE-1 of Section II, Part D of the ASME code.
- 2) The modulus of elasticity, E , evaluated at T_{low} , is obtained by linear interpolation from Table TM-1 of Section II, Part D of the ASME code.
- 3) The maximum allowable stress intensity, S_m , evaluated at T_{high} , is obtained by linear interpolation from Table I-14.2 of Appendix I of the ASME code.
- 4) The maximum strain is calculated as

$$\Delta\epsilon_{\text{max}} = \alpha \Delta T / (1 - \nu)$$

where ν = Poisson's ratio = .3

- 5) The modified maximum equivalent strain is calculated as

$$\Delta\epsilon_{\text{mod}} = \Delta\epsilon_{\text{max}}$$

- 6) The equivalent stress factor is calculated as

$$K_c = \begin{cases} 1 & \text{if } \Delta\epsilon_{\text{mod}} E < 3 S_m \\ \Delta\epsilon_{\text{mod}} E / (3 S_m) & \text{otherwise} \end{cases}$$

- 7) The multiaxial plasticity and Poisson ratio adjustment factor, K_v , are obtained by entering K_c into a fit to Fig. T-1432-3 of the ASME code.
- 8) The total strain range, ϵ_t , is

$$\epsilon_t = K_v \Delta\epsilon_{\text{mod}}$$

- 9) The total strain range is entered into the tables associated with the design fatigue curve of Fig. T-1420-1 of the ASME code for the appropriate material. These tables give design limits for cycles as a function of strain range for various temperatures. Log-log interpolation is used to obtain cycles as a function of strain range. Linear interpolation is used for temperature interpolation.

1. Treatment of HT-9 and Martensitic Steel

One of the problems with the ASME Appendix T treatment of low cycle fatigue at elevated temperatures is that this treatment only applies to four materials. None of these four materials has a composition similar to that of HT-9. Also, none of these four materials is similar to the high silicon martensitic steel recommended by the Russians for use with lead-bismuth coolant. In contrast, the ASME low cycle fatigue treatment in Subsection NB of section III is limited to temperatures below 700 - 800 °F; but it is applicable to broad classes of steels, including one category for ferritic steels and another category for austenitic steels. Thus, when analyzing the subassembly load pads in a PRISM-type ATW, one can find fatigue limits for HT-9 using an approach not applicable for elevated temperatures; or one can find elevated temperature fatigue limits for another material, such as 316 stainless steel; but one can not find elevated temperature limits for HT-9.

To estimate fatigue limits for HT-9 at elevated temperatures, it was decided to analyze the load pads with the Appendix T treatment using 316 stainless steel properties and then to multiply the allowable number of cycles, N_c , by a factor, f_{HT-9} , to get the allowable number of cycles for HT-9. Thus:

$$N_c(HT-9) = f_{HT-9} N_c(316 \text{ ss})$$

To obtain a value for f_{HT-9} cases were evaluated for both HT-9 and 316 ss using the Section III, Subsection NB treatment and no correction for elevated temperature operation. In these cases the allowable number of cycles for HT-9 tended to be about one sixth of the allowable number of cycles for 316 ss. Thus, the value used for f_{HT-9} is 1/6. The same treatment was used for the high silicon martensitic steel as for HT-9.

E. Coolant Heat Transfer Coefficient

An important parameter in the calculation of the thermal strain in the structure is the value used for the coolant heat transfer coefficient. For many components, such as the above core load pads, the intermediate heat exchanger shell, the intermediate heat exchanger upper tube sheet rim, and the steam generator upper tube sheet, the evaluation of the coolant heat transfer coefficient was straightforward. A standard forced convection heat transfer correlation was used. On the other hand, for the outlet plenum wall, there is not much forced convection. Therefore, the natural circulation correlation of Churchill and Chu⁶ was used for the outlet plenum wall.

Table 2 lists the coolant heat transfer coefficients used in calculating transient structural temperatures. The coolant heat transfer coefficients for sodium are higher than those for lead-bismuth because of the higher thermal conductivity of sodium. Also, in the case of the subassembly duct wall and above core load pads, the lead-bismuth design used a larger pin spacing, giving a larger coolant flow area and a larger hydraulic diameter. This was done to reduce the subassembly pressure drop, but increasing the coolant flow area and hydraulic diameter also decreases the coolant heat transfer coefficient. A lower coolant heat transfer coefficient tends to insulate the structure from

coolant temperature changes and reduces the magnitude of transient structure surface temperature changes.

Table 2
Coolant Heat Transfer Coefficients Used in Structure Temperature Calculations

Case	Coolant	Coolant Heat Transfer Coef., w/m ² -K
Above core load pads	Na	1.23 x 10 ⁵
	Pb-Bi	1.388 x 10 ⁴
Outlet Plenum Wall	Na	3993
	Pb-Bi	1778
IHX shell	Na	16,082
IHX tube sheet rim	Na	45,169
Steam generator tube sheet	steam	5500

IV. RESULTS

A. Loss of Beam Transient

Loss of beam transients were run for both the sodium cooled design and the lead-bismuth cooled design. In both cases the initial coolant temperature rise in the hottest core channel was 164 K, and the average coolant temperature rise was 139 K. In these transients, the external source from the beam dropped instantly from full power to zero. The pumps were not tripped.

Figure 3 shows the powers and flow for sodium cooled cases. Lead-bismuth cooled cases give similar powers and flows. It can be seen from Figure 3 that the power drops almost instantly from nominal power to a much lower value after the loss of the beam. Then the power drops slowly toward decay heat levels. In the early part of the transient, the power drops significantly lower with a k effective of .92 rather than .975. Most of the cases in this report were run with a k effective of .92. The impact of the degree of subcriticality is discussed in section IV B below.

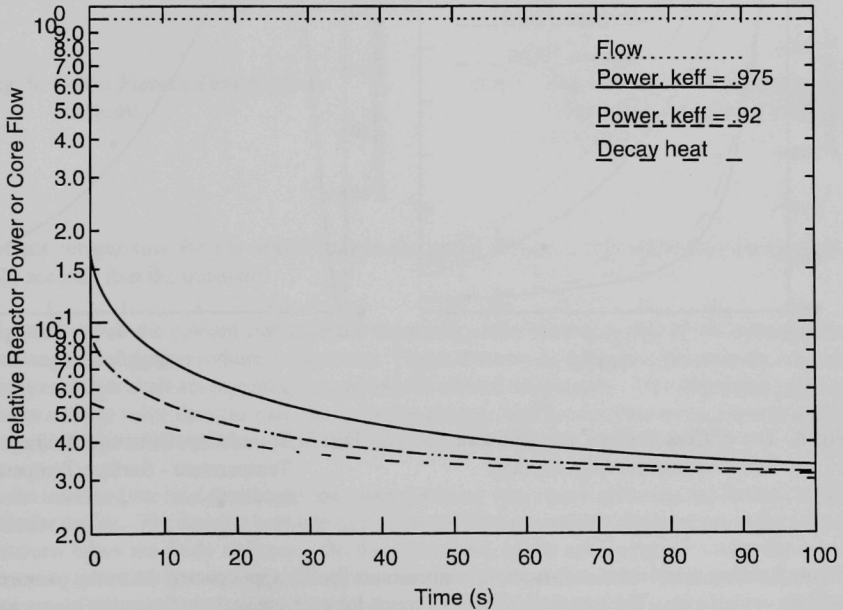


Fig. 3. Normalized Power and Flow, Beam Loss, No Pump Trip

Figure 4 shows the coolant and structure temperatures at the position of the subassembly above core load pads in the hottest subassembly for the sodium cooled case. Because of the high coolant heat transfer coefficient, the structure surface temperature is near the coolant temperature. During much of the transient, the average structure temperature calculated with 20 radial nodes in TSLAB is about 20 K lower than the value calculated with two radial nodes in SASSYS-1. Figure 5 shows the difference between the structure average temperature and the structure surface temperature at the position of the above core load pads. This difference peaks at 66 K at two seconds into the transient. Results for lead-bismuth coolant are similar, except the difference between the structure surface temperature and the coolant temperature is larger because of the lower coolant heat transfer coefficient. This leads to a smaller difference between the structure average temperature and the surface temperature.

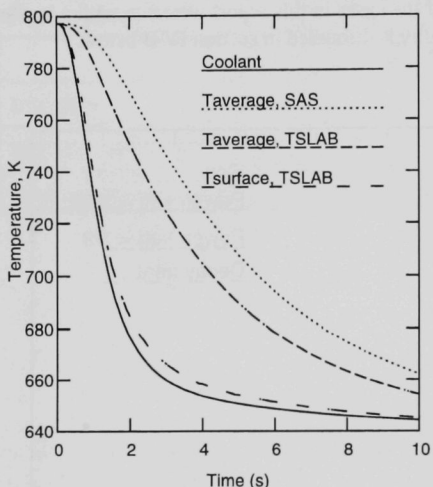


Fig. 4. Top of Core Coolant and Structure Temperatures (sodium coolant)

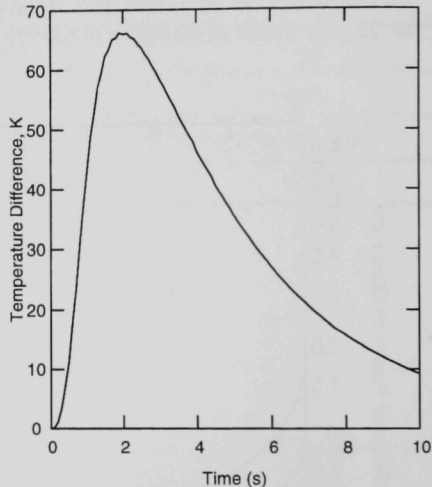


Fig. 5. Top of Core Structure Average Temperature - Surface Temperature (sodium)

Figure 6 shows the coolant and structure temperatures for the upper part of the outlet plenum in the sodium cooled case. The transient involves a much longer time scale in the outlet plenum than in the subassembly because it takes time for the core flow to mix with the large volume of coolant in the outlet plenum. The difference between the coolant temperature and the wall surface temperature is larger than in the subassembly duct wall case because of the lower coolant heat transfer coefficient in the outlet plenum case. Figure 7 shows the difference between the average temperature and the

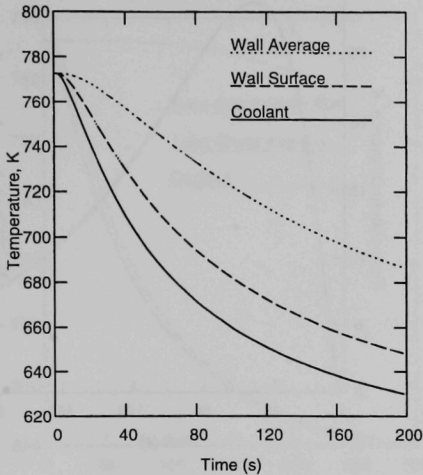


Fig. 6. Outlet Plenum Temperatures (sodium)

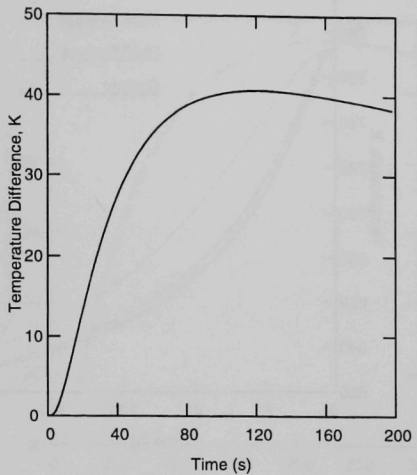


Fig. 7. Outlet Plenum Structure Average Temperature - Surface Temperature (sodium)

surface temperature for the vessel liner in the outlet plenum. This difference peaks at 41 K at 121 seconds into the transient.

Figure 8 shows the coolant and structure temperatures for the upper part of the intermediate heat exchanger shell for the sodium coolant case. Figure 9 shows the difference between the intermediate heat exchanger shell average temperature and the surface temperature. This difference peaks earlier and at a lower value than the case for the outlet plenum wall because the outlet plenum wall is one inch thick whereas the intermediate heat exchanger shell is only 3/4 inch thick.

In the intermediate heat exchanger, the tubes penetrate tube sheets at the top and bottom of the heat transfer region. The spacing between tubes is small enough that the temperatures in the tube sheets between tubes are fairly uniform. On the other hand, at the outer edge of a tube sheet is a rim containing no tube penetrations. The tube sheet is welded to the shell. The total thickness of the region with no tube penetrations plus the shell is up to .0635 m (2.5 inches), which is significantly more than the distance between tube penetrations (.75 inches). Thus, the thermal strains in the tube sheet rim can be significantly higher than the strains between tube penetrations. To estimate the thermal strains in the upper tube sheet rim in the sodium cooled case, a TSLAB case was set up with

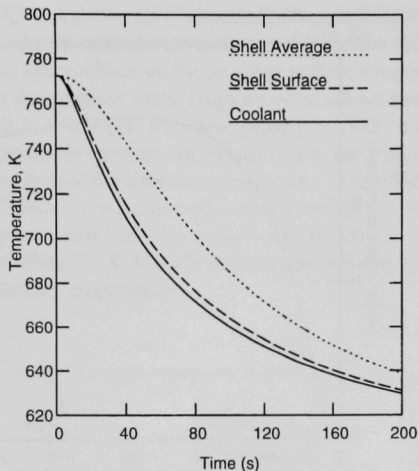


Fig. 8. IHX Shell Temperatures (sodium)

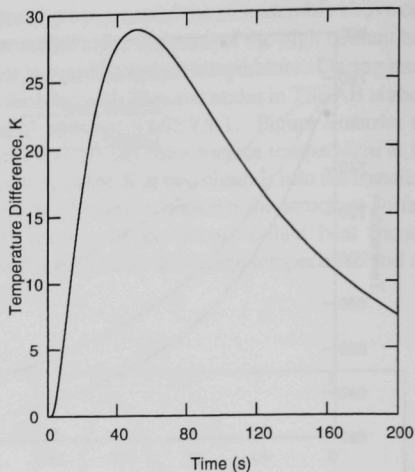


Fig. 9. IHX Shell Average Temperature - Surface Temperature (sodium)

a steel slab .0635 m thick to model the tube sheet rim. Also, a TCYLNDR case was set up to model the interior of the tube sheet around a tube. The intermediate loop coolant temperatures leaving the tube section were used for the coolant temperatures in the TSLAB and TCYLNDR cases. At the back of the intermediate heat exchanger, near the vessel wall, the coolant is almost stagnant. Therefore, a region of stagnant sodium plus the steel vessel liner were included in the TSLAB model. Figure 10 shows the tube sheet rim temperatures calculated for the sodium cooled case. The coolant heat transfer coefficient in the tubes is high enough that the metal surface temperature is not much higher than the coolant temperature. The rim is thick enough that the rim average temperature drops only slowly in the transient. Figure 11 shows the difference between the tube sheet rim outer temperature and the tube sheet average temperature. This difference peaks at a value of 114 K at 219 seconds.

In the lead-bismuth cooled case, there is no intermediate heat exchanger. Instead there is a steam generator inside the vessel where the intermediate heat exchanger would be. For the purposes of this report, a once through steam generator similar to the ALMR mod B design was used. The tubes in the steam generator are larger and farther apart than in the intermediate heat exchanger. Thus the highest transient thermal strain in the tube sheet is due to the difference between the temperature at the inner surface of a tube and the average tube sheet temperature. Thermal strains in the tube sheet rim are smaller. A TCYLNDR model was set up for the upper tube sheet interior around a tube. The

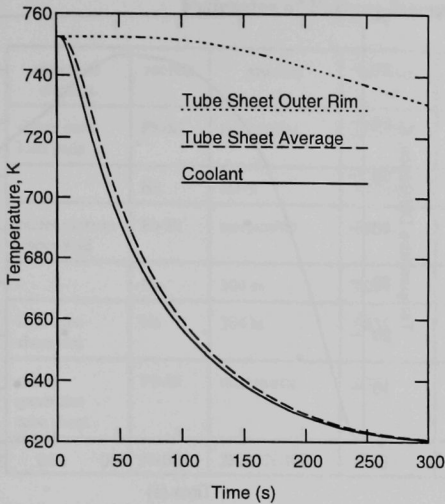


Fig. 10. IHX Upper Tube Sheet Temperatures (sodium)

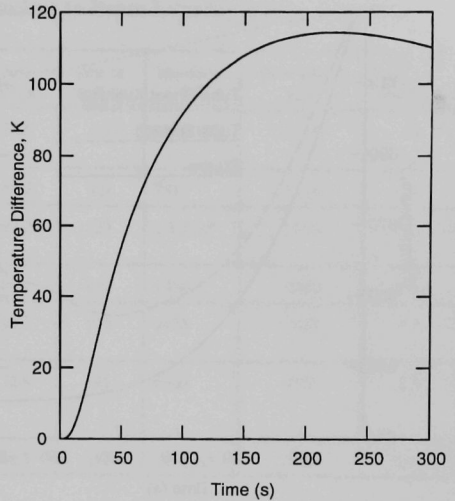


Fig. 11. IHX Tube Sheet Rim Outer Temperature - Tube Sheet Average Temperature (sodium)

detailed steam generator model in SASSYS-1 was used to obtain steam temperatures in the tubes at the top where they penetrate the upper tube sheet. Figure 12 shows the steam generator upper tube sheet temperatures. The steam heat transfer coefficient is lower than the sodium heat transfer coefficient in the sodium cooled intermediate heat exchanger case, so the difference between the structure surface temperature and the coolant temperature is larger in the steam generator case. Figure 13 shows the difference between the tube sheet average temperature and the tube inner surface temperature for the steam generator case. The temperature difference peaks at 73 K at 191 seconds into the transient.

Table 3 summarizes the peak structure temperature differences and gives the corresponding fatigue results for both sodium cooled and lead-bismuth cooled systems. Subassemblies are normally left in the core for three or four years, so with sodium coolant the fatigue damage to the above core load pads is not acceptable unless some mitigation action is taken. With lead-bismuth coolant, the above core load pad design is adequate if the frequency of beam interruptions is no worse than the LANSCE data. With either coolant the damage to the outlet plenum upper wall is within acceptable bounds with the specified frequency of interruptions. If the plant is expected to operate for 30 years, then the fatigue damage to the intermediate heat exchanger tube sheet rim requires mitigation action.

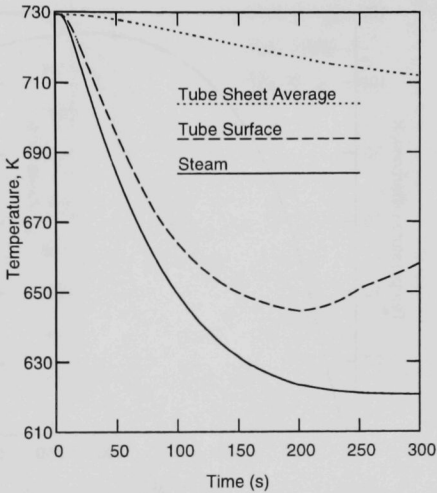


Fig. 12. Steam Generator Upper Tube Sheet Temperatures (Pb-Bi)

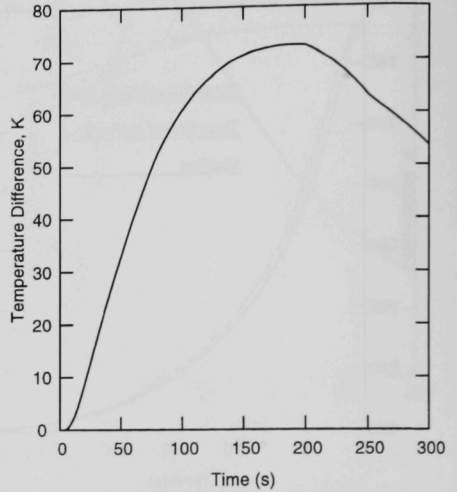


Fig. 13. Tube Sheet Average Temperature - Surface Temperature (Pb-Bi)

The largest uncertainty in these calculations is the actual frequency of interruptions of the accelerator. The ATW accelerator has not been designed or built, so the actual reliability of the beam is unknown.

It might appear from the results in Table 3 that from a thermal fatigue point of view lead-bismuth is a better coolant for the ATW design than sodium, but out of necessity the designs are different. In particular, in order to avoid a large coolant pressure drop in the core, the lead-bismuth design uses smaller pins with more space between pins. If the sodium cooled design used the same small pins and larger space between pins, then for the same pumping power the sodium cooled device could have a significantly higher coolant flow rate, leading to a smaller coolant temperature rise across the core and significantly lower thermal strains in the transient.

Table 3
Estimates of Fatigue Damage Due to Beam Interruptions

structural element	coolant	material	thickness (m)	peak ΔT (K)	time of peak (s)	allowable cycles	interruptions/year	years of operation
above core load pads	Pb-Bi	martensitic	.0056495	44.6	3.2	6.8×10^4	14,200	4.8
	Na	HT-9	.0056495	66.2	1.9	7517	14,200	.53
outlet plenum upper wall	Pb-Bi	martensitic	.0254	27.0	127	1.7×10^5	2019	84+
	Na	304 ss	.0254	40.7	121	10^6+	2019	495+
IHX tube sheet rim	Na	304 ss	.0635	114.3	219	2475	1489	1.7
steam generator tube sheet	Pb-Bi	martensitic	.0753	72.8	191	8100	1551	5.2
	Na	2 1/4 Cr-1 Mo	.0753	68.3	211	2.6×10^5	1489	175

B. Impact of the Degree of Sub-Criticality

As mentioned previously, most of the cases run for this report were run with a blanket k effective = .92 in order to obtain conservative results. At the beginning of a re-fuelling cycle k effective might be .975. For comparison, one case was run with a k effective of .975. This was a sodium cooled case identical to the case previously described except for the value of k effective. Figure 14 shows the influence of k effective on the difference between the above core load pad average temperature and the structure surface temperature at this location. With k effective equal to .975, the peak temperature difference is 62.2 K instead of 66.2. This is not a large difference, but the fatigue curves are very non-linear. The difference of 4 K in peak temperature difference results in increasing the allowable number of cycles from 7500 to 12000. Downstream of the core subassemblies, in the outlet plenum and beyond, the transient temperature changes caused by changing k effective from .92 to .975 are less than 1 K. Thus, the main fatigue consequence is in the subassemblies.

C. Beam Interruption Frequency Design Limits

Based on the results in Table 3, it is possible to obtain design limits for beam interruption frequencies. These limits are shown in Table 4, assuming a four year lifetime in the blanket for subassemblies, and assuming a 30 year life for the intermediate heat exchangers and the steam generators.

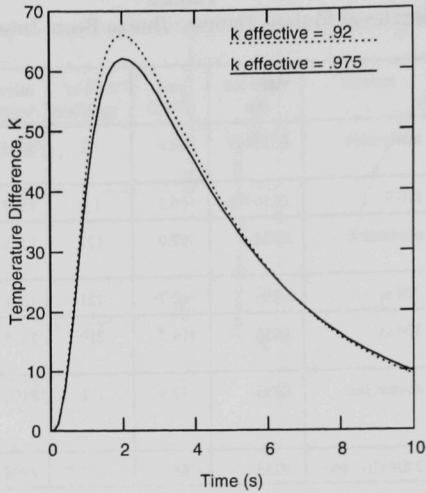


Fig. 14. Influence of k Effective on the Difference Between the Top of Core Structure Average Temperature - Surface Temperature

Table 4
Allowable Beam Interruption Frequencies for Current Blanket Designs

interruption duration	allowable interruptions per year, Pb-Bi coolant	allowable interruptions per year, Na coolant
2 s or more	17,000	1900
3 minutes or more	270	80

V. MITIGATION OPTIONS

A number of mitigation options can be considered to solve thermal fatigue problems. These mitigation options tend to fall in one of three categories. One category is reducing the frequency of beam interruptions. The second category is to reduce the amplitude of the temperature perturbations. The third category is to stretch out the time scale of the temperature perturbations.

A. Improve the Reliability of the Accelerator

Improving the reliability of the accelerator and reducing the frequency of beam interruptions would extend the lifetime of components subjected to thermal fatigue. Improving the reliability of the accelerator would also improve the average effective utilization of the ATW, increasing the rate at which waste is transmuted and increasing the amount of electricity produced. Using multiple accelerators, with each providing a fraction of the required beam current is another solution. If two accelerators were used, with each providing half of the beam current, then losing one accelerator beam would only cut the blanket power in half. The amplitude of the thermal strain cycle would be cut in half. The frequency of interruptions might be doubled; but because of the non-linearity of the fatigue curves, the allowable number or cycles would be increased by an order of magnitude or more.

Figure 15 shows results of a beam interruption in one accelerator if two accelerators are used. These results are for the steam generator tube sheet in the lead-bismuth cooled case. Losing half of the beam current reduces the peak temperature difference from 73 K to 32 K and increases the tube sheet lifetime to more than 50 years.

B. Sudden Return to Power

One way that one might consider reducing thermal fatigue effects is to recover from a beam interruption and go immediately back up to power. Figure 16 shows some results from investigating this option. A beam interruption occurred at $t = 0$. Then the beam was restored immediately to full power at various times. As seen in this figure, if the beam is restored in less than two seconds, then there is some reduction in the peak temperature difference causing thermal strains at the above core load pads. On the other hand, if the beam is restored at two seconds or later, there is no reduction in the peak temperature difference. Thus, the beam needs to be restored in less than two seconds in order to help the thermal fatigue situation at the above core load pads.

Another aspect of the return to power is that a sudden return to power can aggravate the thermal fatigue situation if the return to power comes after the temperatures have had time enough to equilibrate. Figure 17 shows the impact on above core load pad temperature differences if power is suddenly restored 30 seconds after the beam loss occurred. The sudden return to power causes a temperature perturbation that is the mirror image of the sudden loss of the beam. This doubles the peak-to-peak thermal strain amplitude. Because of non-linearities in the fatigue curves, doubling the peak-to-peak strain amplitude can reduce the allowable number of cycles by a factor of ten or more. Thus, any return to power after about two seconds of beam loss will have to be gradual rather than sudden. The time required to increase the power will have to be at least as long as the beam was off.

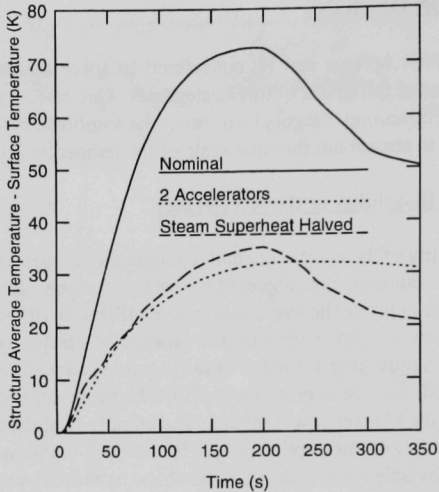


Fig. 15. Temperature Differences in the Steam Generator Tube Sheet of a Lead-Bismuth Cooled ATW, Mitigation Options

C. Pump Trip

In a critical liquid metal cooled reactor, the pumps are normally tripped when a scram occurs. This is to limit thermal shock in various structures. In an ATW the pumps and turbines could be tripped whenever a beam interruption occurs. Figures 18 and 19 show the consequences of a beam loss followed 0.25 seconds later by a pump trip for the sodium cooled design. The pump trip does not completely eliminate thermal strain in the above core load pads, but it does reduce the strain considerably. Figures 20 and 21 show the outlet plenum wall results for the same transient. The pump trip almost eliminates thermal strains downstream of the core. When the beam is lost and the pumps trip, the power drops faster than the flow, so the coolant temperature in the core drops. The time scale for the drop in the coolant temperature is comparable to the time scale for thermal response in the above core load pads, so a moderate temperature difference between the structure and the coolant develops. In contrast, after the pumps trip the coolant flow rate into the outlet plenum is small; and the time scale for coolant mixing in the outlet plenum is longer than the time scale for thermal response of the outlet plenum wall. Thus, little temperature difference develops between the outlet plenum wall and the coolant in the outlet plenum.

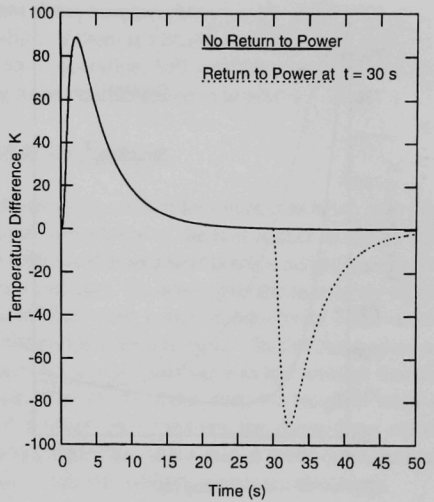
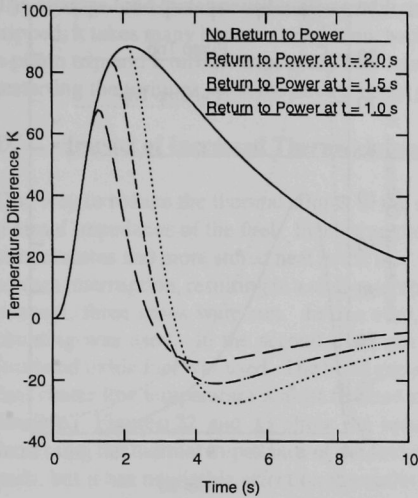


Fig. 16. Influence of Early Return to Power on the Top of Core Difference Between the Structure and the Coolant Temperatures

Fig. 17. Impact of a Sudden Return to Power After Temperatures Have Equilibrated

There are two problems with tripping the pumps and turbines every time a beam interruption occurs in an ATW. One problem is a safety problem, and the other problem relates to the average load factor or utilization. If one trips the pumps a few hundred thousand times during the lifetime of a plant, then the probability is fairly high that sometime the beam will be lost, the pumps will be tripped, the beam will be restored, but the pumps will not be restarted. This results in an accident equivalent to a loss-of-flow accident. The ALMR critical reactor was designed to survive a loss-of-flow accident, with negative reactivity feedback reducing the power to a level that natural circulation flow could handle. In the ATW, negative reactivity feedback has little impact on the power level. Thus in a sodium cooled ATW, a loss-of-flow accident could lead to a core meltdown. For the lead-bismuth cooled reactor design considered here, there would be enough natural circulation flow that core melting would not occur.

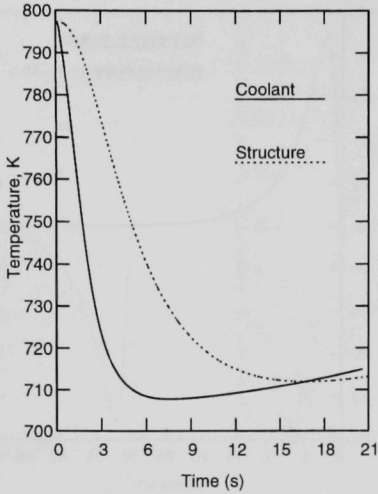


Fig. 18. Top of Core Temperatures After a Loss of Beam with a Pump Trip

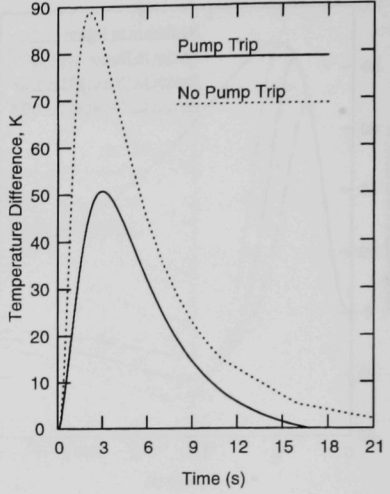


Fig. 19. Top of Core Structure Temperature - Coolant Temperature after a Loss of Beam

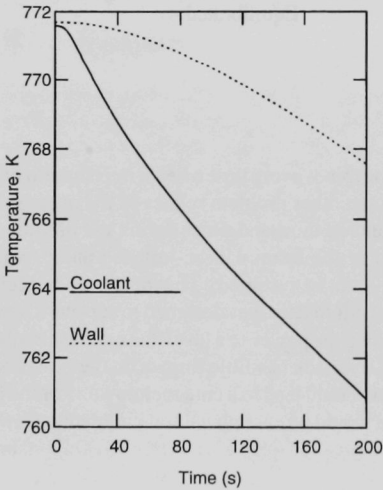


Fig. 20. Outlet Plenum Temperatures After a Loss of Beam with a Pump Trip

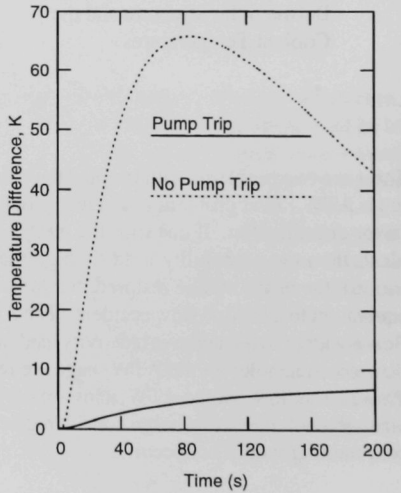


Fig. 21. Outlet Plenum Wall Temperature - Coolant Temperature After a Loss of Beam

The average load factor or utilization problem comes about because every time that the turbines are tripped, it takes many hours to bring them back on-line. If there is a beam interruption, followed by a pump trip and a turbine trip, every half hour or so of operation, followed by a number of hours restarting the turbines, then the device is not going to be operating very much of the time.

D. Impact of Increased Thermal Impedance of the Fuel

One way to reduce the thermal strains in the structures when a beam loss occurs is to increase the thermal impedance of the fuel. Increasing the thermal impedance of the fuel results in higher fuel temperatures and more stored heat in the fuel. The additional stored heat is released gradually after a beam interruption, resulting in a slower temperature transient. To investigate the feasibility of this concept, three cases were run. In one case, a metal fuel with a high-conductivity bond to the cladding was used. In the second case, gas bonded oxide fuel was used. In the third case, an insulated oxide fuel was used. The bond gap conductance in the third case was low enough that the fuel center line temperature almost reached melting. These three cases span the range of what is feasible. Figures 22 and 23 show the results of a beam loss transient for these three cases. Increasing the thermal impedance of the fuel pin does help the thermal strain in the above core load pads, but it has negligible effect on the outlet plenum wall and other downstream structures.

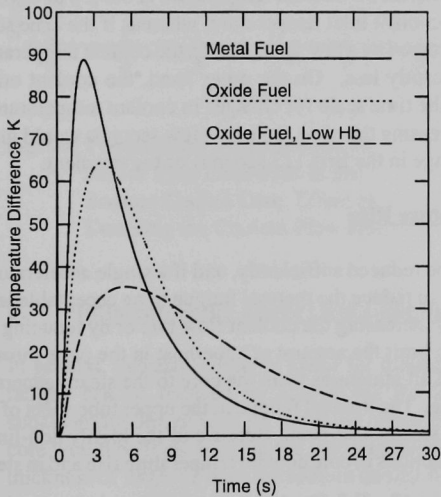


Fig. 22. Top of Core Structure Temperature Minus Coolant Temperature

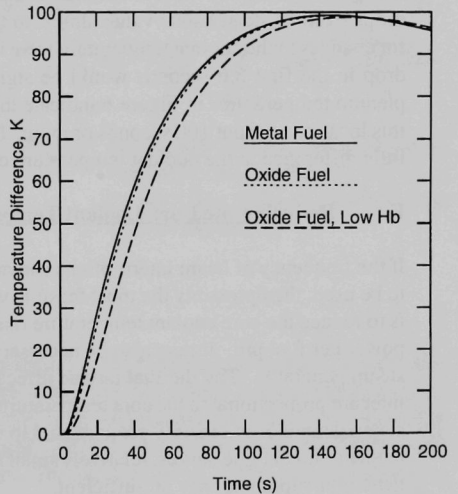


Fig. 23. Outlet Plenum Wall Temperature Minus Coolant Temperature

These results can be understood by considering the relevant time scales. The time scale for heat transfer from a metal fueled pin to the coolant is a fraction of a second. For a gas bonded oxide fuel pin the time scale is in the 1-2 second range. For the insulated oxide fuel of the third case the relevant heat transfer time scale is a few seconds. Thus, increasing the thermal impedance of the fuel pins can add a few seconds to the time scale for coolant temperature changes. The peak thermal strain in the structure resulting from a beam loss is approximately proportional to the coolant temperature change during a period equal to the thermal time constant of the structure. The thermal time constant, τ , of the structure is given by

$$\tau = \pi\delta^2/(4\alpha)$$

where

$$\alpha = k/(\rho C)$$

ρ = density of the structure

C = heat capacity of the structure

δ = thickness of the structure.

For the above core load pads, this time constant is about 5.6 seconds, whereas for the vessel liner in the outlet plenum the time constant is 113 seconds. One can see from the coolant temperatures in Figure 4 that in the first 5.6 seconds of the transient the coolant temperature at the top of the core drops from its steady-state value almost to the coolant inlet temperature, whereas if the time scale for changes in the coolant temperature were increased by a few seconds then the coolant temperature drop in the first 5.6 seconds would be significantly less. On the other hand, the coolant outlet plenum temperatures in Figure 6 indicate that the time scale for changes in coolant temperature at this location is about 100 seconds or more. Increasing this time scale by a few seconds would make little difference in the coolant temperature change in the first 113 seconds of the transient.

E. Reducing the Core Coolant Temperature Rise

If the frequency of beam interruptions can not be reduced sufficiently, and if a single accelerator is to be used, then probably the most feasible way to reduce the thermal fatigue to an acceptable level is to reduce the core coolant temperature rise by increasing the coolant flow rate or by reducing the power per fuel pin. It may also be necessary to limit the amount of superheat in the once-through steam generator. The thermal fatigue effects in all structures from the core to the steam generator inlet are proportional to the core temperature rise. The thermal fatigue in the upper tube sheet of the steam generator are mainly proportional to the steam superheat. Because of the highly non-linear nature of the fatigue curves, relatively small reductions in core coolant temperature rise and in steam generator superheat may be sufficient.

One of the curves in Figure 15 shows the results of reducing the steam generator superheat from 103 K to 52 K in the lead-bismuth cooled case. The peak temperature difference in the tube sheet is reduced from 73 K to 35 K.

Figures 24 and 25 show temperature difference results when the coolant flow rate in the primary and intermediate coolant loops is doubled in the sodium cooled case. This cuts the steady-state core temperature rise in half. Doubling the coolant flow rates solves the thermal fatigue problems in both the above core load pads and the intermediate heat exchanger tube sheet rim.

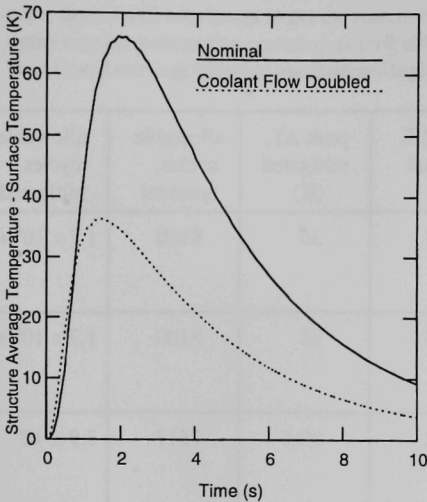


Fig. 24. Temperature Differences in the Above Core Load Pads in the Sodium Cooled Case, Effect of Doubling the Coolant Flow Rate

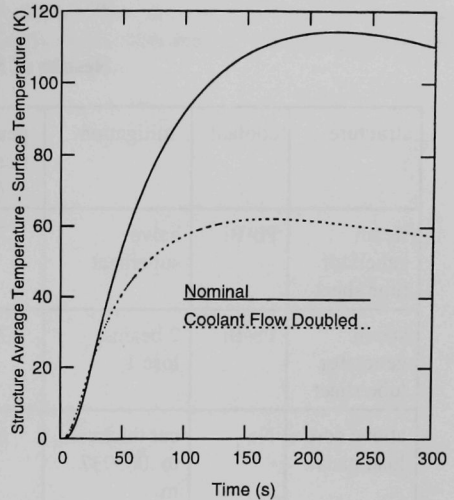


Fig. 25. Temperature Differences in the IHX Tube Sheet Rim in the Sodium Cooled Case, Effect of Doubling the Coolant Flow Rate

F. Eliminating the Above Core Load Pads

In general, thermal fatigue is lower for thinner structures. Thus, subassembly duct wall thermal fatigue can be reduced by eliminating the above core load pads and using a free-flowing subassembly design with no clamping above the core. The subassembly wall thickness above the core would be reduced from the load pad thickness of .005652 m to the nominal subassembly wall thickness of .003937 m in the sodium cooled design. This reduces the peak temperature difference in the structure from 66.2 K to 49.5 K. The allowable number of cycles is increased by about a factor of 5. If the LANSCE interruption frequency data of Table 1 is used, then the subassemblies will still not last in the core for three years, but only minor improvements in the accelerator reliability would be required to achieve an in-core lifetime of 3-4 years.

G. Summary of Mitigation Results

A summary of the results of some of the mitigation actions discussed above is given in Table 5. In all of the cases listed in the table, except for eliminating the above core load pads, the mitigation action is more than sufficient to accommodate the LANSCE interruption frequencies of Table 1.

Table 5
Results of Mitigation Actions

structure	coolant	mitigation	peak ΔT , nominal (K)	peak ΔT , mitigated (K)	allowable cycles, nominal	allowable cycles, mitigated
steam generator tube sheet	Pb-Bi	halve superheat	72.8	35	8100	$1.7 \times 10^6 +$
steam generator tube sheet	Pb-Bi	2 beams, lose 1	72.8	32	8100	$1.7 \times 10^6 +$
above core load pads	Na	cut thickness to .003937 m	66.2	49.5	7517	3.9×10^4
above core load pads	Na	double coolant flow	66.2	35.9	7517	$1.7 \times 10^6 +$
IHX tube sheet rim	Na	double coolant flow	114.3	62.3	2475	7.3×10^5

VI. FUTURE WORK

An aspect of beam interruption consequences in which additional work is needed is consideration of the average load factor or utilization and its effect on power generation and transmutation of waste. Any time that the beam is lost for more than about one second, the beam must be re-started slowly to limit thermal shock to the blanket. Also, if the beam is lost long enough that the turbine trips, then it will take hours to get the turbine back online. Thus, there is some incentive to consider options to keep the turbine running as long as possible after a beam loss in hopes that the power can be restored without tripping the turbine.

VII. SUMMARY AND CONCLUSIONS

Thermal fatigue in the blankets due to temperature transients caused by beam interruptions is a serious problem for current ATW blanket designs if beam interruption frequencies observed for the LANSCE accelerator are assumed. Allowable beam interruption frequencies are obtained for current sodium cooled and lead-bismuth cooled blanket designs. If the allowable beam interruption frequencies can not be met, or if they can not be guaranteed before the design and construction of the blanket, then blanket design options exist that can accommodate higher beam interruption frequencies.

APPENDIX A. VERIFICATION OF THE TSLAB CODE

For validation of the TSLAB code, a problem with a known analytic solution was run. This was a case of a slab that started at a uniform temperature. The surface temperature was suddenly changed and then held at a constant value. For this case the initial temperature was 700 K, and the surface temperature was dropped to 600 K at time zero. The exact solution for this case is

$$T(x, t) = 700 - 100 \operatorname{erfc} \left(\frac{x}{2 \sqrt{\frac{\rho C}{k} t}} \right)$$

This case was run in TSLAB for a steel slab with a thickness of 0.02 meters, 20 node intervals, $k = 21.81$, and $\rho C = 4.779 \times 10^6$. The coolant temperature was dropped from 700 at $t = 0$ to 600 at $t = 10^{-4}$ and held there. For this case $h_c = 10^8$ and $h_{\text{sink}} = 0$. An initial time step of .001 second was used for 10 steps, followed by .01 second for 9 steps and .1 second for 30 more steps. The results for this case are shown in Figure A1 for three times. The TSLAB results agree almost exactly with the exact analytic solution.

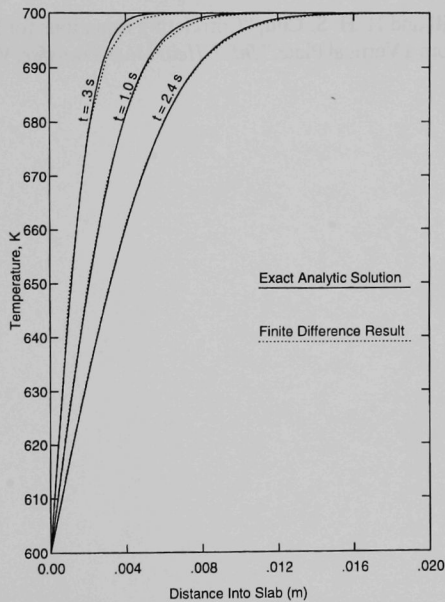


Fig. A1. Comparison of Exact and Finite Difference Solutions for a Slab Temperature Problem

REFERENCES

1. M. Eriksson et al., "Reliability Assessment of the LANSCE Accelerator System," presented at the workshop on the utilization and reliability of high power accelerators, MITO, Japan (October 13-15, 1998).
2. P. M. Magee, A. E. Dubberley, A. J. Lipps and T. Wu, "Safety Performance of the Advanced Liquid Metal Reactor," *Proceedings of ARS '94 International Topical Meeting on Advanced Reactors Safety*, Pittsburgh, Pennsylvania, Vol. 2, pp. 826-833 (April 1994).
3. W. Yang, personal communication (March 21, 2000).
4. F. E. Dunn, F. G. Prohammer, D. P. Weber and R. B. Vilim, "The SASSYS-1 LMFBR Systems Analysis Code," *ANS International Topical Meeting on Fast Reactor Safety*, Knoxville, TN, pp. 999-1006 (April 1985).
5. The American Society of Mechanical Engineers, *1998 ASME Boiler & Pressure Vessel Code, an International Code*, Section III, Subsection NH, Appendix T, Article T-1432.
6. S. W. Churchill and H. H. S. Chu, "Correlating Equations for Laminar and Turbulent Free Convection from a Vertical Plate," *Int. J. Heat Mass Transfer*, Vol. 18, pp. 1323-1329, 1975.

Distribution for ANL-01/05

Internal:

J. E. Cahalan, RAE, 208
D. C. Crawford, NT, ANL-West
F. E. Dunn, RAE, 208 (6)
P. J. Finck, RAE, 208
C. Grandy, RAE, 208
M. R. Hale, IPD-TIS, 203
J. E. Herceg, RAE, 208
D. J. Hill, RAE, 208
R. N. Hill, RAE, 208
H. S. Khalil, RAE, 208
J. J. Laidler, CMT, 205
M. E. Mehaffey, RAE, 208 (2)
D. R. Pedersen, RAE, 208
J. Roglans, RAE, 208
T. A. Taiwo, RAE, 208
RAE Division (10)

External:

ANL-East Library (Bldg. 203)
ANL-West Library (IS/AW-752)
DOE-OSTI

E. Arthur, Los Alamos National Laboratory, Los Alamos, NM 87545
M. Cappiello, Los Alamos National Laboratory, Los Alamos, NM 87545
R. Sheffield, Los Alamos National Laboratory, Los Alamos, NM 87545
G. VanTuyle, Los Alamos National Laboratory, Los Alamos, NM 87545

John Herczeg, DOE, 19901 Germantown Rd., Room A-243, Germantown, MD 20874-1290
Frank Goldner, DOE, 19901 Germantown Rd., Room A-283, Germantown, MD 20874-1290

ARGONNE NATIONAL LAB WEST



3 4444 00038103 8